ELSEVIER

Chemical Geology 208 (2004) 233–245

CHEMICAL GEOLOGY
INCLUDING
ISOTOPE GEOSCIENCE

www.elsevier.com/locate/chemgeo

# The solubility of Pt in liquid Fe-sulfides

K.L. Pruseth*, H. Palme

*Institut für Mineralogie und Geochemie, Universität zu Köln, Zülpicher Strasse 49b, D-50674 Köln, Germany*

**Abstract**

The partitioning of Pt between liquid sulfides with approximately stoichiometric FeS and Pt–Fe alloys was experimentally studied. Experiments were conducted in corundum crucibles enclosed in evacuated quartz vials heated to 1100, 1200 and 1300 °C. Starting materials were Pt metal and sulfides of $Fe_{70}S_{30}$ composition. Run products were coarse Pt–Fe alloys and quenched sulfide melts crystallized to FeS and dendrites of Pt–Fe alloys. All phases were analyzed with the electron microprobe (EMP) and the composition of average sulfide melt was calculated. The Pt contents of sulfide melts increase from 0.01 to nearly 10 at.% with S contents increasing from 45 to 50 at.%. Metal/liquid sulfide atom ratios of Pt range from 3 to 1400. After recalculating the data to unit Pt activity in metal, rather constant Pt contents in sulfides were obtained for S-rich systems with $f_{S_2}$ above $10^{-4}$ atm. On average, 13.1 ± 6 at.% Pt (or 53 ± 22 wt.% Pt) would be dissolved in liquid sulfides in equilibrium with Pt at unit Pt activity. By using the Pt solubilities in sulfides obtained here and those in silicates measured by Borisov and Palme [Geochim. Cosmochim. Acta 61 (1997) 4349] and by assuming the $f_{O_2}$ to be defined by the QFM buffer, Pt liquid sulfide/silicate partition coefficients, $D_{Pt}^{Sul/Sil}$, were calculated. These partition coefficients are several orders of magnitude higher than those experimentally determined. The most likely reason is the formation of Pt-rich nuggets in partition experiments.


*Keywords:* Solubility; Partitioning; Liquid sulfide

## 1. Introduction

The elements Ru, Rh, Pd, Os, Ir and Pt are designated as platinum group elements (PGE). To these six elements, Re and Au are often added and these eight elements are collectively designated as highly siderophile elements (HSE). The concentrations of the HSE in the Earth's mantle are less than a percent of their CI-chondritic abundances (e.g., McDonough and Sun, 1995). The origin of the HSE in the crust–mantle system of the Earth has been a matter of debate for many years. It now appears that the HSE were delivered to the Earth with an unfractionated late accretionary component after the end of core formation. The validity of this "late veneer" model is primarily based on two arguments:

(1) The relative abundances of the HSE in the Earth's mantle are essentially chondritic, as shown by a large number of analyses of upper mantle rocks (Morgan et al., 2001 and references). In detail, there is some variability in HSE mantle abundances, but in view of the large geochemical

* Corresponding author. Present address: Geochemistry Laboratory, School of Environmental Sciences, Jawaharla Nehru University, New Delhi, India.

*E-mail address:* palme@min.uni-koeln.de (K.L. Pruseth).

0009-2541/$ - see front matter © 2004 Elsevier B.V. All rights reserved.
doi:10.1016/j.chemgeo.2004.04.014

differences among the HSE, the approximately chondritic ratios in upper mantle rocks are remarkable and suggest incorporation of HSE as a single component after core formation had ceased. The metal/silicate partition coefficients of HSE are extremely high, but different from each other (Borisov and Palme, 2000). Recent results by Holzheid et al. (2000) from high pressure experiments have shown that Pt and Pd metal/silicate partition coefficients do not decrease with increasing pressure as required by models where the mantle abundances of HSE are established by core/mantle equilibrium (Murthy, 1991).

(2) The Os-isotopic composition of upper mantle rocks requires a chondritic Re/Os ratio from the beginning of the Earth (Meisel et al., 1996). Given the initial chondritic relative abundances of HSE in the Earth's mantle, deviations from chondritic ratios must reflect igneous processes, e.g., melting and/or crystallization.

The pattern of HSE in the Earth's crust is quite different from that of the mantle. It is fractionated with Os and Ir depletions by factors of around 100 and increasing abundances in the sequence Ru, Pt, Pd and Re with Re reaching approximately mantle abundances (Schmidt et al., 1997; Schmidt and Palme, 1998; Peucker-Ehrenbrink and Jahn, 2001). This is, except for Re, a pattern of increasing abundance with decreasing melting point. This type of pattern is frequently encountered in rocks derived from the terrestrial mantle by partial melting (Barnes et al., 1985). The same pattern is also characteristic of lunar basalts (Neal et al., 2001). The origin of this type of fractionated pattern is unclear. Differences in solubility of HSE in silicates (Barnes et al., 1985), in sulfides (e.g., Brügmann et al., 2000) or in both (Rehkämper et al., 1999), have been suggested. Involvement of sulfide melts would require large differences between liquid sulfide/liquid silicate partition coefficients for Ir and Os on one hand and Pt and Pd, with their much higher crustal abundances, on the other hand. Such differences are not obvious in experimentally determined sulfide/silicate partition coefficients (see Peach et al., 1994; Fleet et al., 1996, 1999). In Table 1, we have documented the enormous spread in experimentally determined Pt sulfide/silicate partition coefficients in the literature. Other HSE partition coefficients show a similar or even larger scatter. With such uncertainties, it is difficult to quantitatively assess the relevance of sulfides for fractionating the PGE.

Table 1
Summary partition coefficients for Pt ($D_{Pt}^{Sul/Sil} \times 10^{-3}$) compiled from Fleet et al. (1996, 1999)

| $D_{Pt}^{Sul/Sil}$ | $f_{O_2}$ | Ni/(Fe+Ni) | PGE (ppm)[a] | References |
|---|---|---|---|---|
| 9.1 | | | | Stone et al. (1990) |
| >1000 | | | | Bezmen et al. (1991) |
| 4.4 | IQF | 0.14 | <200 | Fleet et al. (1991) |
| 25 | IQF | 0.17 | >39,000 | |
| 15 ± 10 | WM | 0.18 | <500 | Fleet et al. (1996) |
| 10 ± 4 | WM | 0.36 | <1000 | |
| 16.5 ± 6.3 | WM | high Ni | <350 | Crocket et al. (1997) |
| 10.5 | | low Ni | | |
| 25 ± 10 | WM | 0.66 | | |
| 1.4 ± 0.4 | CCO | 0.02 | <300 | Fleet et al. (1999) |
| 3.9 ± 1.8 | IQF | 0.61 | <300 | |

The PGE concentrations are that in the respective sulfide melts.
[a] Amount of PGE in the starting material.

In the present work, an attempt is made to better understand the interaction of the HSE with sulfide liquids. This is done by studying the solubility of Pt in sulfide liquids as a function of temperature and sulfide composition. From a comparison of solubilities of Pt in liquid sulfides and in liquid silicates, we will derive liquid sulfide/liquid silicate partition coefficients which will then be compared with experimentally determined sulfide/silicate partition coefficients.

## 2. Experimental

### 2.1. Starting materials

The starting sulfide composition (Fe/S = 70:30 wt.%) corresponds to the eutectic between pure iron and troilite on the Fe–S binary (Kullerud et al., 1969). Powders of Fe metal of 99.99% purity and elemental S of better than 99.999% purity in the eutectic proportions were sealed under a vacuum ( ≈ 8 mbar) with an oxygen–hydrogen torch. After keeping the charge for a day at 200 °C in a horizontal furnace, it was finally annealed at 500 °C for 4 days. Iron-rich starting materials were obtained by mixing the required amount of Fe to this base composition and grinding

under acetone. Sulfur-rich compositions were made by adding extra S and by annealing for further 4 days at 500 °C in evacuated quartz ampoules. Platinum foil of 0.1 mm thickness and 99.99% purity was used for the solubility experiments.

### 2.2. Experimental procedures and results

All solubility experiments were conducted in 5 × 7 mm evacuated silica tubes. The charge containing approximately 30 mg of sulfide powder and 3 mg of Pt foil was placed in a 3 × 4 mm cylindrical corundum crucible which was sealed under vacuum in a quartz capsule (Fig. 1). At the temperatures of the present experiments, PGEs and Fe non-reactively invade the quartz tube, thus rendering the use of the corundum crucible imperative. A quartz rod of ≈ 4 mm diameter was placed above the corundum crucible to check the loss of sample powder to the vacuum line and to prevent heating up of the charge during necking and sealing procedures. Additionally, a piece of wet cotton was kept wrapped around the charge during the sealing process. Four to five such charges in a small basket of platinum wires were kept hanging from a long Pt wire in a vertical furnace (HTRV 70-250, GERO, Neuhausen) at the desired temperatures. At the completion of the experiments, the charges were quenched by dropping them into a jug of cold water, at the lower end of the furnace tube. Temperature was constant within a length of approximately 6 cm in the hot zone of the furnace and was controlled within ± 2 °C by an EUROTHERM temperature controller. A $Pt_{94}Rh_6$–$Pt_{70}Rh_{30}$ thermocouple calibrated against the melting point of gold was used to monitor the temperature inside the furnace.

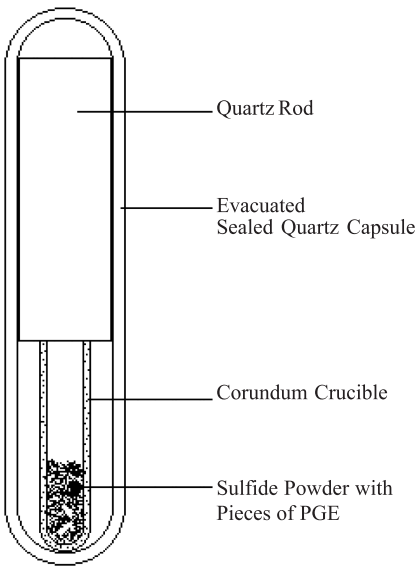


Fig. 1. Configuration of the experimental charge.

After quenching, the experimental products were recovered by breaking open the silica capsules. The pieces of quenched melt and the remnant PGE metal were mounted in araldite for making polished sections. The sulfide melt is highly unquenchable and crystallization of a Pt–Fe alloy phase cannot be avoided.

The duration of the experiments varied from 2 to 49 h. Platinum is dissolved in the sulfide melt, but there is at the same time diffusion of Fe from the melt into the Pt foil (see below).

#### 2.2.1. Sulfides

The sulfide melt was found to be highly non-quenchable. Additionally, although the charges were quenched by dropping directly into ice-cold water, the corundum crucible—inside the quartz capsule and separated by an annular stretch of vacuum—lost heat comparatively slowly and a perfect quenching was impossible. The distribution of the exsolved Pt–Fe blebs was non-uniform on a small scale. Therefore, the quenched sulfide liquids were analyzed by an Electron Probe Microanalyzer (EPMA, JEOL SUPERPROBE JXA-8900RL) using a broad beam of 30 μm. An accelerating potential of 20 kV and a beam current of 15 nA were used. Sufficiently large areas (150 × 150 to 300 × 300 μm) were mapped to ensure representative analyses. In Fig. 2, quenched sulfide melt, dendrites of metal phase and of remnant Pt foil are shown. Thus two generations of dendrites are present: non-eutectic metal (i.e. original Pt foil) represented by bright large exsolution-like blebs and eutectic FePt alloys as small dendritic assemblages. For each sample, at least five different areas were scanned. The presence of bubbles in some samples required larger areas to be scanned. Analyses with sums falling outside the range of 98–102% were discarded. Good agreement among the analyses for

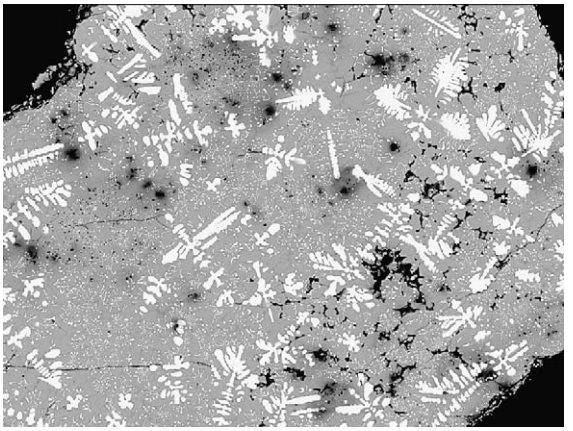

Fig. 2. Backscattered electron image of Pt29. There are two generations of PtFe metals. Large brighter dendrites are remnants of the Pt foil. Fine light gray dendrites have crystallized as Pt–Fe metals from liquid sulfides on quenching (456 × 343 μm).

small and large areas is indicative of the representativity of the method.

*2.2.2. Metals*

The compositions of the coexisting metal phases were determined under the same conditions but using a focussed beam. In early experiments with short-run durations (2 h), metal was found to be strongly zoned, later experiments with longer durations showed little or no zoning. The profiles across the Pt foils for two different experimental durations, at 1200 and 1300 °C, are plotted in Fig. 3. It is clear that at 1300 °C homogenization occurs within an interval of 2 h. The sulfide melts are also found to be compositionally uniform over different areas. In earlier short duration experiments and in some experiments at 1200 °C the composition of the metal is zoned (Fig. 3). In these experiments, the composition at its contact with the melt has been taken to be the equilibrium metal composition in order to calculate the partition coefficients. In two experiments (Pt26 and Pt27) at 1200 °C, the metal foils did not attain homogeneity, even after 49 h. Grains of Fe powder, added in these charges to obtain a very Fe-rich starting composition, alloyed with the Pt foils and virtually shielded them from the sulfide melts. A gray rim of Fe-rich alloy phase was observed around the Pt foils. Compositions of individual tiny Fe grains were found to be similar to those of the rims at their contacts with the sulfide melt whereas within the enclosed Pt foil there existed a steep gradient of Fe from the periphery down to the center. The presence of trace amounts of sulfides along fine cracks, in some cases, within the Pt foil near its contact with the sulfide melt made the measurements difficult. Therefore, several profiles were measured for each sample and the compositions of spots within 10 μm from the boundary with minimum S and maximum Fe were selected as the equilibrium compositions.

## 3. Results and discussion

Results of the Pt solubility experiments at 1100, 1200 and 1300 °C are summarized in Table 2. Experimental results are converted to at.% in Table 3. In Tables 2–4, samples are arranged according to increasing ambient partial pressures of $S_2$ in sulfides calculated from the coexisting sulfide melt–alloy compositions, as discussed below. In addition, metal/sulfide weight ratios of Fe and Pt are listed. The data provided in Table 2 are the averages of five or more compositions, individually determined by summing up each of the scan areas and calculating averages and standard deviations (in parentheses). In a few experiments with high metal to sulfide ratios, it was not possible to demarcate even five representative areas of 5 × 5 pixels, the minimum permissible size for mapping; however, at least three areas have been used for each of the samples.

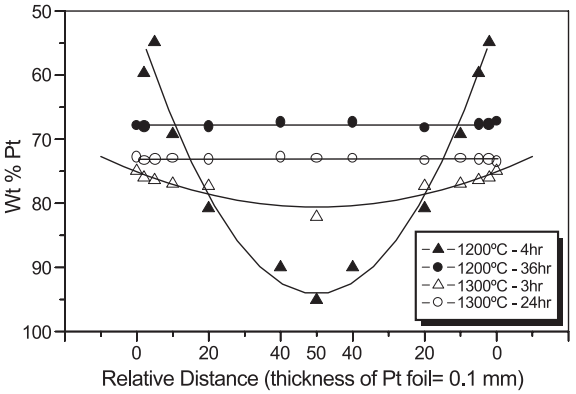


Fig. 3. Compositional profile across Pt foils after experimentation.

Table 2
Composition of equilibrium pairs of sulfide melt and Pt–Fe alloy in wt.% and duration of experiments

| Sample | Sulfide melt (wt.%) | | | Metal alloy (wt.%) | | | Duration (h) |
|---|---|---|---|---|---|---|---|
| | Fe | S | Pt | Fe | S | Pt | |
| *1100 °C* | | | | | | | |
| Pt30 | 67.95 (0.32) | 32.03 (0.32) | 0.03 (0.01) | 89.52 (0.12) | 0.05 (0.01) | 10.44 (0.12) | 72 |
| J7 | 66.89 (0.37) | 33.20 (0.34) | 0.11 (0.01) | 45.43 (0.89) | 0.01 (0.03) | 54.57 (0.86) | 8 |
| J6 | 66.94 (0.14) | 32.82 (0.26) | 0.08 (0.01) | 36.05 | 0.07 | 63.88 | 4 |
| J5 | 67.10 (0.32) | 32.78 (0.38) | 0.12 (0.01) | 33.95 | 0.06 | 65.99 | 12 |
| S4 | 67.20 (0.29) | 32.59 (0.25) | 0.13 (0.01) | 32.95 | 0.01 | 67.04 | 4 |
| Pt34 | 65.93 (0.17) | 33.86 (0.17) | 0.21 (0.01) | 32.02 | 0.06 | 67.92 | 72 |
| Pt32 | 59.99 (0.03) | 39.90 (0.02) | 0.11 (0.02) | 13.41 | 0.09 | 86.49 | 72 |
| Pt33 | 61.03 (0.19) | 38.91 (0.19) | 0.06 (0.01) | 20.20 | 0.10 | 79.70 | 72 |
| *1200 °C* | | | | | | | |
| Pt4 | 66.64 (0.23) | 32.68 (0.28) | 0.08 (0.01) | 69.59 | 0.01 | 30.40 | 4 |
| J10 | 66.82 (0.02) | 32.86 (0.01) | 0.13 (0.01) | 56.04 (0.34) | 0.03 (0.01) | 43.93 (0.34) | 2 |
| J9 | 66.62 (0.26) | 33.22 (0.29) | 0.22 (0.02) | 37.10 (1.48) | 0.02 (0.03) | 62.88 (1.48) | 2 |
| Pt8 | 66.18 (0.22) | 33.42 (0.16) | 0.40 (0.07) | 32.75 (0.66) | 0.05 (0.02) | 67.19 (0.67) | 36 |
| Pt3 | 65.49 (0.38) | 33.84 (0.39) | 0.67 (0.05) | 28.15 (1.07) | 0.13 (0.02) | 71.72 (1.09) | 4 |
| Pt7 | 64.52 (0.09) | 34.39 (0.08) | 1.09 (0.01) | 26.02 (0.31) | 0.05 (0.02) | 73.93 (0.30) | 36 |
| Pt21 | 60.57 (0.36) | 34.39 (0.18) | 5.05 (0.54) | 15.42 (0.17) | 0.09 (0.01) | 84.49 (0.16) | 15 |
| Pt20 | 61.32 (0.08) | 34.52 (0.07) | 4.16 (0.14) | 14.90 (0.25) | 0.06 (0.04) | 85.03 (0.29) | 15 |
| Pt18 | 57.28 (0.29) | 34.38 (0.45) | 8.34 (0.69) | 14.73 (0.14) | 0.02 (0.01) | 85.25 (0.16) | 15 |
| Pt13 | 49.68 (1.39) | 32.32 (0.02) | 18.00 (1.41) | 15.63 | 2.42 | 81.95 | 19 |
| Pt19 | 57.35 (0.89) | 34.47 (0.26) | 8.17 (1.07) | 13.72 (0.05) | 0.08 (0.02) | 86.20 (0.06) | 15 |
| Pt14 | 52.47 (0.95) | 33.05 (0.11) | 14.48 (1.07) | 11.97 (0.30) | 0.09 (0.07) | 87.94 (0.29) | 19 |
| Pt12 | 39.03 (0.45) | 29.02 (0.15) | 31.95 (0.60) | 10.81 (0.23) | 0.09 (0.03) | 89.10 (0.22) | 19 |
| Pt26 | 68.13 (0.39) | 31.83 (0.40) | 0.04 (0.02) | 98.96 (0.10) | 0.06 (0.01) | 0.98 (0.11) | 49 |
| J9-r | 67.20 (0.75) | 32.70 (0.73) | 0.10 (0.02) | 96.61 (0.07) | 0.07 (0.02) | 3.32 (0.08) | 2.5 |
| J10-r | 67.98 (0.59) | 31.98 (0.60) | 0.04 (0.01) | 96.46 (0.15) | 0.05 (0.02) | 3.49 (0.15) | 2.5 |
| Pt27 | 66.98 (0.24) | 32.91 (0.26) | 0.10 (0.03) | 93.32 (0.06) | 0.03 (0.02) | 6.66 (0.08) | 49 |
| *1300 °C* | | | | | | | |
| Pt11 | 63.77 (1.50) | 34.36 (0.38) | 1.87 (1.13) | 23.47 (0.29) | 0.11 (0.03) | 76.42 (0.28) | 24 |
| Pt25 | 64.03 (0.43) | 34.31 (0.23) | 1.66 (0.24) | 23.13 (0.34) | 0.10 (0.02) | 76.78 (0.36) | 20.5 |
| Pt5 | 64.94 (0.29) | 34.22 (0.28) | 0.83 (0.28) | 22.37 (0.61) | 0.00 (0.04) | 77.63 (0.63) | 3 |
| Pt24 | 62.78 (0.13) | 34.11 (0.10) | 3.11 (0.05) | 20.55 (0.36) | 0.06 (0.05) | 79.39 (0.38) | 20.5 |
| Pt10 | 60.83 (0.11) | 34.62 (0.05) | 4.55 (0.12) | 19.38 (0.33) | 0.06 (0.03) | 80.56 (0.35) | 24 |
| Pt22 | 53.86 (0.18) | 33.42 (0.22) | 12.72 (0.41) | 13.59 (0.23) | 0.04 (0.04) | 86.36 (0.24) | 20.5 |
| Pt23 | 57.22 (0.10) | 34.27 (0.20) | 8.51 (0.31) | 13.18 (0.23) | 0.09 (0.03) | 86.73 (0.24) | 17.5 |
| Pt15 | 42.06 (1.05) | 29.64 (1.05) | 28.30 (1.05) | 12.21 | 0.10 | 87.69 | 8 |
| Pt16 | 52.26 (1.02) | 33.06 (0.72) | 14.68 (1.64) | 11.81 (0.41) | 0.09 (0.04) | 88.10 (0.41) | 8 |
| Pt17 | 51.23 (1.05) | 32.88 (0.45) | 15.89 (1.33) | 11.67 (0.20) | 0.09 (0.06) | 88.25 (0.19) | 17.5 |
| Pt28 | 65.89 (0.09) | 33.71 (0.09) | 0.39 (0.01) | 98.79 (0.22) | 0.02 (0.01) | 1.18 (0.24) | 24 |
| Pt29 | 66.31 (0.67) | 33.39 (0.68) | 0.29 (0.02) | 92.65 (0.15) | 0.05 (0.02) | 7.31 (0.17) | 24 |

Numbers in brackets—standard deviation of the analysis; missing errors indicate that concentrations were obtained from rim compositions of traverses through PtFe alloys.

In many experiments (Table 3), the sum of Fe and Pt atoms approximately equals the number of S atoms (Fe + Pt ~ S). This suggests that the stable Pt species is PtS. The apparent metal/sulfide melt partition coefficients (by weight) for Pt are decreasing with increasing temperature ranging from 300 to 1400 at 1100 °C; from 5 to 300 at 1200 °C, and from 3 to 100 at 1300 °C (Table 3). Experiments with, less than 50 at.% Fe have significantly lower apparent metal/sulfide partition coefficients (Table 3).

Table 3
Compositions of sulfide melt and metal alloy recast into at.%, ratios of concentrations of Pt and Fe in metal to those in liquid sulfide (by weight) ($D^{Metal/Sulfide}$) and activity coefficient and activity of Pt and Fe calculated according to Gudmundsson and Holloway (1993)

| Sample | Sulfide melt (at.%) | | | Metal (at.%) | | | $D^{Metal/Sulfide}$ (by weight) | | Log $\gamma_{Pt}^{Metal}$ | Log $a_{Pt}^{Metal}$ | Log $\gamma_{Fe}^{Metal}$ | Log $a_{Fe}^{Metal}$ |
|---|---|---|---|---|---|---|---|---|---|---|---|---|
| | Fe | S | Pt | Fe | S | Pt | Pt | Fe | | | | |
| *1100 °C* | | | | | | | | | | | | |
| Pt30 | 54.91 | 45.08 | 0.01 | 96.69 | 0.09 | 3.23 | 390 | 1.32 | − 5.63 | − 7.11 | − 0.01 | − 0.02 |
| J7 | 53.62 | 46.36 | 0.03 | 74.40 | 0.02 | 25.58 | 479 | 0.68 | − 3.01 | − 3.60 | − 0.44 | − 0.57 |
| J6 | 53.93 | 46.06 | 0.02 | 66.21 | 0.21 | 33.58 | 779 | 0.54 | − 2.29 | − 2.76 | − 0.75 | − 0.93 |
| J5 | 54.01 | 45.96 | 0.03 | 64.11 | 0.21 | 35.68 | 554 | 0.51 | − 2.12 | − 2.56 | − 0.84 | − 1.03 |
| S4 | 54.19 | 45.78 | 0.03 | 63.17 | 0.04 | 36.79 | 528 | 0.49 | − 2.05 | − 2.48 | − 0.88 | − 1.08 |
| Pt34 | 52.76 | 47.19 | 0.05 | 62.09 | 0.21 | 37.70 | 328 | 0.49 | − 1.97 | − 2.39 | − 0.93 | − 1.14 |
| Pt32 | 46.32 | 53.66 | 0.03 | 34.99 | 0.42 | 64.59 | 761 | 0.22 | | | | |
| Pt33 | 47.38 | 52.61 | 0.01 | 46.78 | 0.40 | 52.82 | 1386 | 0.33 | | | | |
| *1200 °C* | | | | | | | | | | | | |
| Pt4 | 53.92 | 46.06 | 0.02 | 88.87 | 0.02 | 11.11 | 366 | 1.04 | − 4.03 | − 4.98 | − 0.08 | − 0.13 |
| J10 | 53.84 | 46.12 | 0.03 | 81.61 | 0.07 | 18.31 | 333 | 0.84 | − 3.30 | − 4.04 | − 0.20 | − 0.29 |
| J9 | 53.49 | 46.46 | 0.05 | 67.30 | 0.06 | 32.65 | 283 | 0.56 | − 2.12 | − 2.60 | − 0.61 | − 0.78 |
| Pt8 | 53.15 | 46.75 | 0.09 | 62.89 | 0.18 | 36.93 | 167 | 0.49 | − 1.81 | − 2.24 | − 0.77 | − 0.97 |
| Pt3 | 52.55 | 47.30 | 0.15 | 57.56 | 0.46 | 41.98 | 107 | 0.43 | − 1.48 | − 1.86 | − 0.99 | − 1.23 |
| Pt7 | 51.72 | 48.03 | 0.25 | 55.04 | 0.19 | 44.77 | 68 | 0.40 | − 1.34 | − 1.69 | − 1.10 | − 1.36 |
| Pt21 | 49.68 | 49.13 | 1.19 | 38.78 | 0.40 | 60.83 | 17 | 0.25 | − 0.62 | − 0.83 | − 1.91 | − 2.32 |
| Pt20 | 50.00 | 49.03 | 0.97 | 37.87 | 0.27 | 61.86 | 20 | 0.24 | − 0.59 | − 0.79 | − 1.96 | − 2.38 |
| Pt18 | 47.91 | 50.09 | 2.00 | 37.62 | 0.07 | 62.31 | 10 | 0.26 | − 0.58 | − 0.78 | − 1.98 | − 2.40 |
| Pt13 | 44.70 | 50.66 | 4.64 | 36.09 | 9.73 | 54.18 | 4.5 | 0.31 | − 0.53 | − 0.72 | − 2.06 | − 2.50 |
| Pt19 | 47.89 | 50.15 | 1.96 | 35.61 | 0.36 | 64.03 | 10.5 | 0.24 | − 0.51 | − 0.70 | − 2.09 | − 2.54 |
| Pt14 | 45.95 | 50.42 | 3.63 | 32.09 | 0.42 | 67.50 | 6.1 | 0.23 | − 0.41 | − 0.58 | − 2.29 | − 2.78 |
| Pt12 | 39.53 | 51.20 | 9.26 | 29.64 | 0.42 | 69.94 | 2.8 | 0.28 | − 0.34 | − 0.50 | − 2.43 | − 2.96 |
| Pt26 | 55.13 | 44.86 | 0.01 | 99.61 | 0.11 | 0.28 | 22.1 | 1.45 | − 5.27 | − 7.68 | 0.00 | 0.00 |
| J9-r | 54.11 | 45.86 | 0.02 | 98.91 | 0.12 | 0.97 | 31.8 | 1.44 | − 5.18 | − 7.13 | 0.00 | 0.00 |
| J10-r | 54.96 | 45.03 | 0.01 | 98.88 | 0.09 | 1.02 | 78.9 | 1.42 | − 5.18 | − 7.15 | 0.00 | 0.00 |
| Pt27 | 53.87 | 46.11 | 0.02 | 97.95 | 0.05 | 2.00 | 64.2 | 1.39 | − 5.07 | − 6.75 | 0.00 | − 0.01 |
| *1300 °C* | | | | | | | | | | | | |
| Pt11 | 51.36 | 48.21 | 0.43 | 51.55 | 0.41 | 48.04 | 40.9 | 0.37 | − 1.04 | − 1.35 | − 1.07 | − 1.36 |
| Pt25 | 51.52 | 48.09 | 0.38 | 51.09 | 0.37 | 48.55 | 46.2 | 0.36 | − 1.02 | − 1.33 | − 1.09 | − 1.38 |
| Pt5 | 52.04 | 47.77 | 0.19 | 50.16 | 0.00 | 49.84 | 93.4 | 0.34 | − 0.98 | − 1.28 | − 1.12 | − 1.42 |
| Pt24 | 51.00 | 48.27 | 0.72 | 47.37 | 0.24 | 52.39 | 25.5 | 0.33 | − 0.86 | − 1.14 | − 1.24 | − 1.56 |
| Pt10 | 49.68 | 49.26 | 1.06 | 45.56 | 0.24 | 54.20 | 17.7 | 0.32 | − 0.79 | − 1.06 | − 1.32 | − 1.66 |
| Pt22 | 46.55 | 50.31 | 3.15 | 35.41 | 0.20 | 64.40 | 6.8 | 0.25 | − 0.46 | − 0.65 | − 1.81 | − 2.26 |
| Pt23 | 47.95 | 50.01 | 2.04 | 34.53 | 0.42 | 65.05 | 10.2 | 0.23 | − 0.44 | − 0.62 | − 1.85 | − 2.31 |
| Pt15 | 41.32 | 50.72 | 7.96 | 32.57 | 0.47 | 66.96 | 3.1 | 0.29 | − 0.39 | − 0.56 | − 1.96 | − 2.45 |
| Pt16 | 45.82 | 50.49 | 3.69 | 31.76 | 0.42 | 67.83 | 6.0 | 0.23 | − 0.37 | − 0.53 | − 2.00 | − 2.50 |
| Pt17 | 45.31 | 50.66 | 4.03 | 31.46 | 0.41 | 68.13 | 5.6 | 0.23 | − 0.36 | − 0.52 | − 2.01 | − 2.51 |
| Pt28 | 52.83 | 47.08 | 0.09 | 99.62 | 0.04 | 0.34 | 3.0 | 1.50 | − 4.49 | − 6.90 | 0.00 | 0.00 |
| Pt29 | 53.23 | 46.70 | 0.07 | 97.70 | 0.09 | 2.21 | 24.8 | 1.40 | − 4.29 | − 5.93 | 0.00 | − 0.01 |

The apparent sulfur contents of the Fe–Pt alloys are, in most cases, at a few hundred ppm (Table 2). It cannot be excluded that this is due to fluorescence from sulfide matrix and/or some S contamination. The high S content in Pt13 is probably the result of the small size of the left over Pt foil and consequent excitation from the surrounding sulfide phase (Table 2).

Reversals were attempted with samples J9 and J10. Both samples were equilibrated with Pt metal in the usual way (Table 2). After the experiment, Pt-containing sulfides were separated from Pt metal

Table 4
Log $f_{S_2}$, calculated as described in the text, log $f_{O_2}$ (QFM buffer), weight fraction of Pt in silicate melt at the $a_{Pt}$ of the experiments and QFM (see text), weight fraction of Pt in sulfide (Table 2), calculated liquid sulfide/liquid silicate partition coefficient ($D_{Pt}^{Sul/Sil}$) and solubility of Pt in sulfide (wt. fraction of Pt in sulfide divided by Pt activity in metal)

| Sample | Log $f_{S_2}$ | Log $f_{O_2}$ QFM | $X_{Pt}^{Silicate}$ [by wt.] | $X_{Pt}^{Sulfide}$ [by wt.] | $D_{Pt}^{Sul/Sil}$ [by wt.] | Solubility, $X_{Pt}^{Sulfide}/a_{Pt}^{Metal}$ |
|---|---|---|---|---|---|---|
| *1100 °C* | | | | | | |
| Pt30 | − 6.03 | − 9.75 | 6.70E − 18 | 2.67E − 04 | 3.99E + 13 | 3500 |
| J7 | − 4.93 | − 9.75 | 2.20E − 14 | 1.14E − 03 | 5.19E + 10 | 4.51 |
| J6 | − 4.22 | − 9.75 | 1.53E − 13 | 8.20E − 04 | 5.36E + 09 | 0.47 |
| J5 | − 4.01 | − 9.75 | 2.37E − 13 | 1.19E − 03 | 5.02E + 09 | 0.44 |
| S4 | − 3.92 | − 9.75 | 2.87E − 13 | 1.27E − 03 | 4.43E + 09 | 0.38 |
| Pt34 | − 3.81 | − 9.75 | 3.55E − 13 | 2.07E − 03 | 5.82E + 09 | 0.51 |
| *1200 °C* | | | | | | |
| Pt4 | − 5.06 | − 8.47 | 4.18E − 15 | 8.30E − 04 | 1.99E + 11 | 79.1 |
| J10 | − 4.73 | − 8.47 | 3.66E − 14 | 1.32E − 03 | 3.60E + 10 | 14.3 |
| J9 | − 3.76 | − 8.47 | 9.98E − 13 | 2.22E − 03 | 2.22E + 09 | 0.88 |
| Pt8 | − 3.37 | − 8.47 | 2.27E − 12 | 4.01E − 03 | 1.77E + 09 | 0.70 |
| Pt3 | − 2.86 | − 8.47 | 5.53E − 12 | 6.68E − 03 | 1.21E + 09 | 0.48 |
| Pt7 | − 2.60 | − 8.47 | 8.15E − 12 | 1.09E − 02 | 1.34E + 09 | 0.53 |
| Pt21 | − 0.67 | − 8.47 | 5.88E − 11 | 5.05E − 02 | 8.58E + 08 | 0.34 |
| Pt20 | − 0.55 | − 8.47 | 6.40E − 11 | 4.16E − 02 | 6.50E + 08 | 0.26 |
| Pt18 | − 0.51 | − 8.47 | 6.56E − 11 | 8.34E − 02 | 1.27E + 09 | 0.51 |
| Pt13 | − 0.31 | − 8.47 | 7.55E − 11 | 1.80E − 01 | 2.38E + 09 | 0.95 |
| Pt19 | − 0.24 | − 8.47 | 7.87E − 11 | 8.17E − 02 | 1.04E + 09 | 0.41 |
| Pt14 | 0.26 | − 8.47 | 1.05E − 10 | 1.45E − 01 | 1.38E + 09 | 0.55 |
| Pt12 | 0.61 | − 8.47 | 1.26E − 10 | 3.19E − 01 | 2.52E + 09 | 1.00 |
| Pt26 | − 5.31 | − 8.47 | 8.27E − 18 | 4.43E − 04 | 5.36E + 13 | 21,000 |
| J9-r | − 5.30 | − 8.47 | 2.94E − 17 | 1.05E − 03 | 3.57E + 13 | 14,200 |
| J10-r | − 5.30 | − 8.47 | 2.85E − 17 | 4.42E − 04 | 1.55E + 13 | 6200 |
| Pt27 | − 5.29 | − 8.47 | 7.00E − 17 | 1.04E − 03 | 1.49E + 13 | 5900 |
| *1300 °C* | | | | | | |
| Pt11 | − 2.01 | − 7.36 | 6.63E − 11 | 1.87E − 02 | 2.82E + 08 | 0.42 |
| Pt25 | − 1.97 | − 7.36 | 7.02E − 11 | 1.66E − 02 | 2.37E + 08 | 0.35 |
| Pt5 | − 1.88 | − 7.36 | 7.82E − 11 | 8.31E − 03 | 1.06E + 08 | 0.16 |
| Pt24 | − 1.59 | − 7.36 | 1.07E − 10 | 3.11E − 02 | 2.89E + 08 | 0.43 |
| Pt10 | − 1.39 | − 7.36 | 1.30E − 10 | 4.55E − 02 | 3.49E + 08 | 0.52 |
| Pt22 | − 0.20 | − 7.36 | 3.32E − 10 | 1.27E − 01 | 3.83E + 08 | 0.57 |
| Pt23 | − 0.09 | − 7.36 | 3.55E − 10 | 8.51E − 02 | 2.39E + 08 | 0.36 |
| Pt15 | 0.16 | − 7.36 | 4.10E − 10 | 2.83E − 01 | 6.90E + 08 | 1.03 |
| Pt16 | 0.27 | − 7.36 | 4.36E − 10 | 1.47E − 01 | 3.37E + 08 | 0.50 |
| Pt17 | 0.31 | − 7.36 | 4.45E − 10 | 1.59E − 01 | 3.58E + 08 | 0.53 |
| Pt28 | − 4.72 | − 7.36 | 1.87E − 16 | 3.93E − 03 | 2.10E + 13 | 31,000 |
| Pt29 | − 4.70 | − 7.36 | 1.75E − 15 | 2.95E − 03 | 1.68E + 12 | 2500 |

and re-homogenized with pieces of iron wire at 1200 °C for 2.5 h. During equilibration, sulfide melts in both cases lost Pt to the iron wires and their composition moved towards the Fe-rich end of the regression line on the plot of concentration of Pt vs. Fe/S (Fig. 4). The samples Pt26 and Pt27 at 1200 °C and Pt28 and Pt29 at 1300 °C are also from experiments with addition of metallic iron, i.e. with three starting phases (Pt metal, Fe metal, sulfide). In Pt26 to Pt29, sulfide was added as powder and Pt as a thin Pt foil, while Fe metal was added in the form of somewhat larger granules. Despite a 49 h run time the Pt foils in Pt26 and Pt27 were not homogeneous, with up to 30 at.% Pt

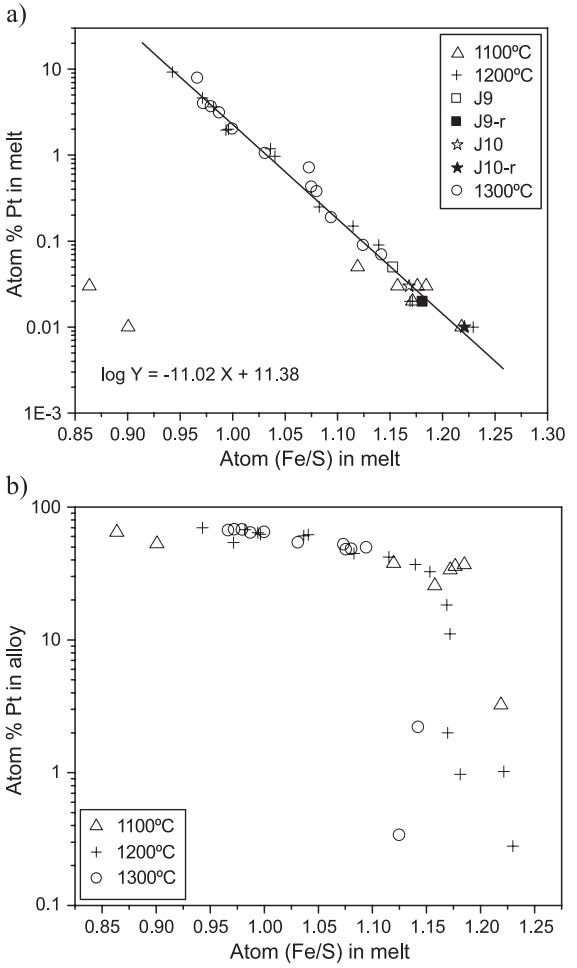


Fig. 4. Concentration of Pt in sulfide melt and Pt–Fe alloy as function of Fe/S of the sulfide melt. S is the residual sulfur after compensating for the Pt dissolved in the melt. J9-r and J10-r are the reversals of J9 and J10, respectively. The two points falling off the regression line in (a) are of the samples, $Pt_{32}$ and $Pt_{33}$ at 1100 °C in which pyrrhotite is a stable phase. The Fe rich runs clearly follow a different trend in (b) implying rapid drop in Pt activity with Fe enrichment.

in the interior and 0.6% Pt at the rim. This must be the result of lower diffusion rates in Fe-rich, Pt-low metals. In Pt28 and Pt29, homogenization of the Pt foils was apparently facilitated by higher temperature. The data for the alloy composition reported in Tables 2 and 3 were taken at the rim of the Pt metal, bordering liquid sulfides. Tiny Fe–Pt alloy metals had the same compositions as the rim suggesting local equilibrium.

### 3.1. Activities of Fe and Pt in metal, and the partial pressure of $S_2$

In Fig. 4a, the log of the concentration of Pt in liquid sulfides is plotted against the Fe/S ratios using the results of all experiments. From the number of S atoms the Pt atoms were subtracted implying that PtS is the stable species of Pt in the sulfide liquid. A straight line in the log $X_{Pt(sulfide)}$ vs. Fe/S plot fits well to all data points, except for Pt32 and Pt33 which contain pyrrhotite, irrespective of the temperature of experimentation:

$$\log X_{Pt(sulfide)} = -11.02(Fe/S)_{(sulfide)} + 11.38$$

The linear scale of Fe/S and the logarithmic scale of Pt indicate a very strong increase of the amount of Pt dissolved in sulfide with increasing S content. A decrease in Fe/S atomic ratio from 1.20 to 0.95, results in an increase in Pt solubility by three orders of magnitude. The strong increase of Pt with increasing S supports the presence of PtS as stable Pt species in the sulfide melt. In Fig. 4b, the Pt contents of the alloy phases are plotted against the Fe/S atom ratio of the sulfide melt. The variation in the Pt contents of the alloy phase is small compared to that in sulfide melt, except for the high Fe runs. Thus the large increase in Pt contents of sulfide liquids reflects the increase of the S content or the sulfur fugacity (see below), variations in Pt of the coexisting metal are not important. In Fig. 5, a combination of Fig. 4a and b, metal/liquid sulfide $K_D$ values are plotted vs. Fe/S ratios. The large range of these partition coefficients is a reflection of the strong increase of Pt in sulfide melt with increasing S fugacity.

Further discussion of the results of the experiments requires the knowledge of (a) the activities of Pt and Fe in the metal alloy and (b) the sulfur fugacity of the system.

(a) The activities of Pt and Fe in metal were calculated from Gudmundsson and Holloway (1993), using their equations:

$$\log\gamma_{Pt} = X_{Fe}^2[B + C(4X_{Fe} - 3)] \quad (1)$$

$$\log\gamma_{Fe} = (1 - X_{Fe})^2[B + C(4X_{Fe} - 1)] \quad (2)$$

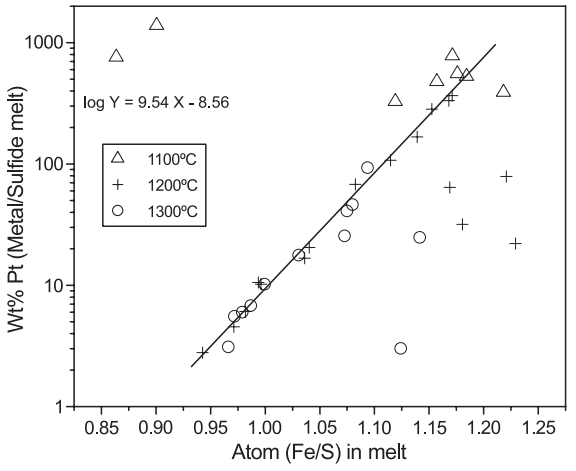


Fig. 5. $D$ = wt.% Pt (metal alloy/sulfide melt) plotted against Fe/S in the sulfide melt. Despite the low Pt concentration (see Fig. 4b), the Fe-rich runs have $D$ values similar to other runs.

where $\gamma_{Pt}$ and $\gamma_{Fe}$ are the activity coefficients of Pt and Fe, respectively, $X_{Fe}$ is the mole fraction of Fe in the alloy, and $B$ and $C$ are temperature-dependent constants. The values for $B$ and $C$ are at 1400 °C: −3.5788 and −0.1510, and at 1300 °C: −4.2019 and −0.3234, respectively. In our calculations, we have used linearly extrapolated values of $B = -4.8250$ and $C = -0.4958$ at 1200 °C, and $B = -5.4481$ and $C = -0.6682$ at 1100 °C. Activity coefficients and activities of Pt and Fe are listed in Table 3.

(b) Sulfur fugacities were calculated from the reaction:

$$\mathrm{Fe} + \frac{1}{2}\mathrm{S_2} = \mathrm{FeS} \tag{3}$$

$$(f_{S_2})^{\frac{1}{2}} = \frac{a_{FeS}}{a_{Fe}K} \tag{4}$$

Thermodynamic data for this reaction were taken from Robie and Hemingway (1995). The Fe activities in metal are those listed in Table 3. The FeS activity of liquid sulfide was assumed to be unity. This is justified in view of the limited range of sulfide compositions. The total range in S (at.%) is between 44.9 and 51.2 (Table 2). The deviation of FeS activities from unity in Fe–S systems discussed here is below 10% (Štofko et al., 1974). The calculated $S_2$ partial pressures are given in the second column of Table 4. According to Eq. (4), variations in $f_{S_2}$ at a given temperature are caused by variations in the activities of Fe in the Pt–Fe alloys, as the activity of FeS is assumed unity. The results at 1200 °C are in reasonable agreement with the results of Štofko et al. (1974) who experimentally determined the activities of Fe and FeS in liquid sulfide by imposing a given $S_2$ partial pressure on a FeS–Fe liquid at 1200 °C.

### 3.2. Metal/sulfide melt partitioning of Pt

The range of metal/liquid sulfide Pt partition coefficients (atoms) from 3 in S-rich systems to 1400 in S-poor systems (Table 3, weight ratios in Fig. 5) is in part a reflection of the variable alloy compositions in equilibrium with sulfides. It is, therefore, useful to normalize the data to a common activity of Pt. The results of this calculation are given in the last column of Table 4, where the atom fractions of Pt in sulfide are divided by the activities of Pt in the coexisting metal. Thus this column gives the amount of Pt in sulfide at unit Pt activity in coexisting metal, i.e., the solubility of Pt in sulfide. In calculating the solubilities, a linear relationship between activity and concentration of Pt in sulfide, i.e., a constant activity coefficient of Pt, or the validity of Henry's law is assumed. In Fe-rich sulfides, this procedure leads to sulfides, with more than 100% Pt (Table 4, column 6). These numbers have no physical meaning, as Henry's law is apparently not obeyed.

For $f_{S_2}$ above $10^{-4}$ atm solubilities are fairly constant, independent of temperature. The average Pt content at unit Pt activity is $13.1 \pm 6$ at.% Pt (or $53 \pm 22$ wt.%). In other words, the coexistence of pure Pt metal and Fe sulfides with sulfur contents from 46 to 51 at.% S imposes about 13 at.% Pt on the coexisting liquid sulfide. Such high Pt contents cannot be obtained in an experiment, as Pt will always form alloys with Fe and thus reducing the Pt activity below unity. At lower S contents where Pt–Fe alloys are the dominant Pt carrying phases the large extrapolations required here lead to unreasonable Pt contents.

In an earlier section, we have concluded from the stoichiometry of the sulfides that Pt is dissolved as PtS and solubilities should therefore depend on sulfur fugacity. The approximately constant Pt solubilities in sulfide melts which are apparently independent of $f_{S_2}$ are the accidental result of increasing Pt solubilities

with increasing S content (Fig. 5) and simultaneously increasing Pt activities in the coexisting alloy. Alternatively Pt is dissolved in liquid sulfide as Pt-metal species.

### 3.3. The Fe–Pt–S ternary

In Fig. 6, we have plotted the Pt solubility results for 1100, 1200 and 1300 °C on Fe–Pt–S ternary diagrams. All three diagrams are very similar. The inserts represent enlarged portions of the sulfide compositions. Coexisting phases are connected by tie lines. The higher the Pt content of the sulfides the more Pt rich is the coexisting metal alloy. The 1100 °C data fit well with the more precise phase diagram recently published by Majzlan et al. (2002). These authors reported four distinct Pt–Fe alloys at 1100 °C, which may also be present at higher temperatures and would thus explain the clustering of data points on the Fe–Pt joins in Fig. 6. The PtFe–$Pt_3Fe$ miscibility gap is probably visible at the 1300 °C data, although Kubaschewski (1982) reported miscibility above ca. 1300 °C for PtFe and above ca. 1350 °C for $Pt_3Fe$. As discussed above, there are six experiments with addition of Fe in the starting materials, four at 1200 °C (Pt26 to Pt29, J9-r and J10-r) and two at 1300 °C (Pt28 and Pt29). These six experiments have all very low Pt in their metal phases and plot very near the Fe–S binary in Fig. 6 (see also Table 3). However, the Pt contents in the sulfide melts of these experiments are not very different from those with significantly higher Pt contents of up to 30% in their metal phase. One possibility is the presence of a three-phase field in the ternary with the Fe–FeS eutectic composition (liquid sulfide), $Pt_1Fe_{99}$ and $Pt_{30}Fe_{70}$ as end members. This could also explain the large change of Pt in metal in the Fe-rich samples mentioned above (see Fig. 6). This is, however, not supported by the data of Majzlan et al. (2002) and the experimental results at 1200 °C (Fig. 6) also do not suggest a major gap in the composition of Fe–Pt alloys.

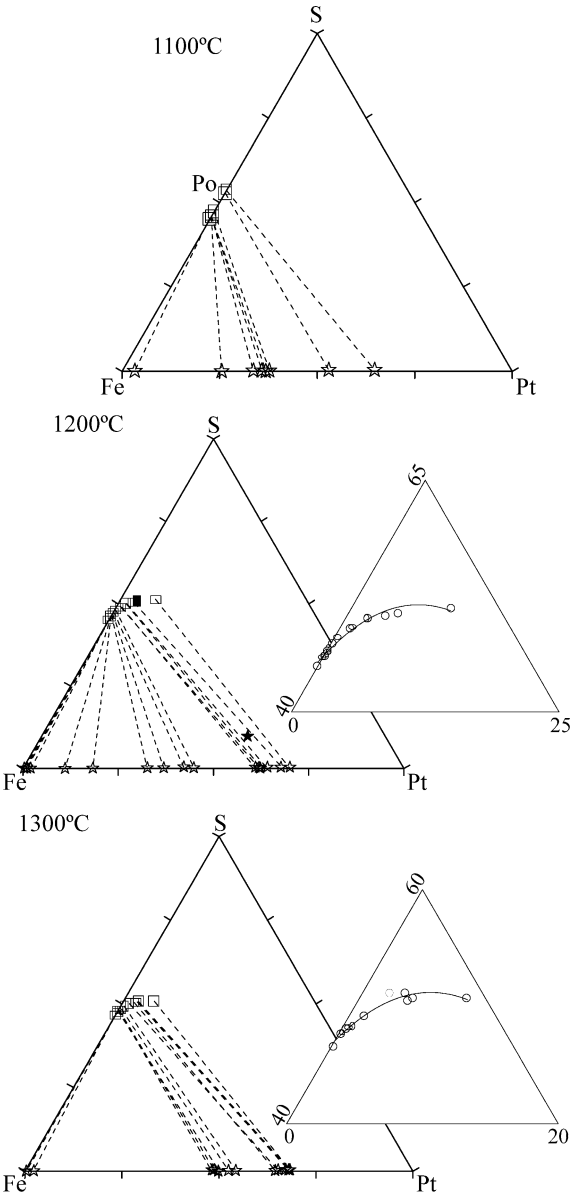


Fig. 6. Compositions of the sulfide melts plotted on the Fe–Pt–S ternary at 1100, 1200 and 1300 °C. Dashed lines are tie lines connecting pairs of equilibrium sulfide and metal compositions. At 1100 °C, for two S-rich starting materials, pyrrhotite appeared as a stable phase. Filled pairs of sulfide and alloy compositions at 1200 °C are those for Pt13 in which the metal composition could not be correctly determined because of very small size of the leftover Pt foil.

### 3.4. Implications for liquid sulfide/liquid silicate partition coefficients

The results of the present study have implications for sulfide/silicate partitioning. Since equilibrium between liquid sulfide and liquid silicates is important for the fractionation of Pt and other PGE in the terrestrial environment, we will attempt to estimate

the partitioning of Pt between these two phases. From the *metal/liquid silicate* partition coefficients of Pt, $D_{Pt}^{Met/Sil}$, calculated from the work of Borisov and Palme (1997) and Ertel et al. (1999), and from the *metal/liquid sulfide* partition coefficients, $D_{Pt}^{Met/Sul}$, determined in this study, it is, in principle possible to estimate *liquid sulfide/liquid silicate* partition coefficients, $D_{Pt}^{Sul/Sil}$.

To facilitate the calculation, we assume the $f_{O_2}$ to be defined by the QFM buffer, representative of the oxygen fugacity in the upper mantle of the Earth. The amount of Pt in silicate melt coexisting with Pt metal ($a_{Pt}=1$) at QFM was calculated from experimental data using regressions of Pt solubility vs. oxygen fugacity given in Borisov and Palme (1997). The resulting Pt contents in the silicate melts are then scaled to the activity of Pt in the present experiments as defined by the Pt–Fe alloys and listed in Table 3, column 11. The calculated Pt contents (by weight) in silicates at QFM and at the Pt activities of the metals of the present experiments are given in Table 4, column 4. These numbers are extremely low reflecting the extremely high metal/silicate partition coefficients and the low Pt activities in the coexisting metals. It is assumed here that Henry's law is valid for PtO in silicate melts, i.e., the activity coefficients of PtO in silicate melt are assumed to be independent of the PtO content. This assumption appears to be justified as both, Borisov and Palme (1997) and Ertel et al. (1999) found a slope of +2 for the correlation of log $X_{Pt}$ vs. log $f_{O_2}$ for a range of Pt values from 100 ppb to 10 ppm. This correlation would break down if there were a major change in the activity coefficient of PtO within this range of Pt contents. In column 5 of Table 4, the weight fraction of Pt in sulfide melt is given (same as in Table 2). The last but one column in Table 4 contains the weight ratios of Pt in liquid sulfide to Pt in liquid silicate. These ratios are the sulfide/silicate partition coefficients at the condition of the experiments and $f_{O_2}$ defined by the QFM buffer.

These calculated liquid sulfide/liquid silicate partition coefficients are very high and depend somewhat on temperature: at 1100 °C around $5\times10^9$, at 1200 °C $10^9$ and at 1300 °C ca. $4\times10^8$. In the Fe-rich experiments, partition coefficients are even higher reflecting the presence of Fe–Pt alloys in sulfides. The high liquid sulfide/liquid silicate partition coefficients of Pt calculated from experimental data on PtS solubility in sulfide and PtO solubility in silicates are not surprising in view of the extremely low solubility of PtO in silicates and the correspondingly high metal/silicate partition coefficients in combination with the comparatively high Pt solubility in Fe sulfides.

As can be seen from Table 1, the experimentally determined partition coefficients of Pt between sulfide and silicate are at least four orders of magnitude lower than those calculated here. The most likely reason is the occurrence of Pt or Pt–Fe metal nuggets that dominate the solubility of Pt in silicate melts at reducing conditions as shown by Borisov and Palme (1997) and Ertel et al. (1999). The latter authors estimated a maximum size of 0.05 μm for the Pt–Rh nuggets present in their experiments. Indirect evidence for tiny Ir metal nuggets is also provided by O'Neill and Nell, 1997 and Lindstrom (1976).

It is likely that nuggets in the Pt and Pt–Rh experiments are present at all oxygen fugacities but are only "visible" at oxygen fugacities below about $10^{-5}$ atm because they would not show up at more oxidizing conditions where the intrinsic PGE level is higher than the PGE level provided by the PGE nuggets. A constant level of about 1 ppm Pt in silicate melt as upper limit of the nugget contamination in the experiments of Borisov and Palme (1997) and Ertel et al. (1999) would correspond to sulfide/silicate partition coefficients of $10^3$–$10^5$ using the weight fraction of Pt in sulfides given in Table 4. In an earlier section, we have shown that sulfide melts with approximately stoichiometric FeS composition would, in equilibrium with Pt metal, contain about 0.53% Pt. A coexisting silicate liquid with 1 ppm Pt dominated by micronuggets would yield a partition coefficient of 5300. This is within the range of experimentally determined sulfide/silicate partition coefficients.

Experimental determinations of Pt sulfide/silicate and Pt metal/silicate partition coefficients are done with pure Pt metal or at least alloys with high Pt contents. This configuration apparently leads to the formation of nuggets enriched in Pt. It is likely that in a natural environment, where pure Pt metal phases are absent such nuggets will not form, implying that experimentally determined sulfide/silicate partition coefficients cannot be used for predicting fractionation of Pt and the noble metals in natural environments.

## Acknowledgements

This study was supported by the Humoldt Gesellschaft through a AvH Fellowship to K.P. Reviews by C. Ballhaus and E. Makovicky were very helpful and led to major changes. **[RR]**

## References

Barnes, S.-J., Naldrett, A.J., Gorton, P., 1985. The origin of the fractionation of platinum-group elements in terrestrial magmas. Chem. Geol. 53, 303–323.

Bezmen, N.I., Ye, G., Brügmann, G.E., Naldrett, A.J., 1991. Mechanism of concentration of platinum-group elements: partitioning between silicate and sulfide melts. Int. Geol. Rev. 33, 784–792.

Borisov, A., Palme, H., 1997. Experimental determination of the solubility of platinum in silicate melts. Geochim. Cosmochim. Acta 61, 4349–4357.

Borisov, A., Palme, H., 2000. Solubilities of noble metals in Fe-containing silicate melts as derived from experiments in Fe-free systems. Am. Mineral. 85, 1665–1673.

Brügmann, G.E., Hanski, E.J., Naldrett, A.J., Smolkin, V.F., 2000. Sulphide segregation in ferropicrites from the Pechenga Complex, Kola Peninsula, Russia. J. Petrol. 41, 1721–1742.

Crocket, J.H., Fleet, M.E., Stone, W.E., 1997. Implications of composition for experimental partitioning of platinum-group elements and gold between sulfide liquid and basaltic melt: the significance of nickel content. Geochim. Cosmochim. Acta 61, 4139–4149.

Ertel, W., O'Neill, H.St.C., Sylvester, P.J., Dingwell, D.B., 1999. Solubilities of Pt and Rh in a haplobasaltic silicate melt at 1300 °C. Geochim. Cosmochim. Acta 63, 2439–2449.

Fleet, M.E., Crocket, J.H., Stone, W.E., 1991. Partitioning of palladium, iridium and platinum between sulfide liquid and basalt melt: effects of melt composition, concentration and oxygen fugacity. Geochim. Cosmochim. Acta 55, 2545–2554.

Fleet, M.E., Crocket, J.H., Stone, W.E., 1996. Partitioning of platinum-group elements (Os, Ir, Ru, Pt, Pd) and gold between sulfide liquid and basalt melt. Geochim. Cosmochim. Acta 60, 2397–2412.

Fleet, M.E., Crocket, J.H., Liu, M., Stone, W.E., 1999. Laboratory partitioning of platinum-group elements (PGE) and gold with application to magmatic sulfide-PGE deposits. Lithos 47, 127–142.

Gudmundsson, G., Holloway, J.R., 1993. Activity–composition relationships in the system Fe–Pt at 1300 and 1400 °C and at 1 atm and 20 kbar. Am. Mineral. 78, 178–186.

Holzheid, A., Sylvester, P., O'Neill, H.St.C., Rubie, D.C., Palme, H., 2000. Evidence for late chondritic veneer in the Earth's mantle from high-pressure partitioning of palladium and platinum. Nature 406, 396–399.

Kubaschewski, O., 1982. Iron-Binary Phase Diagrams. Springer-Verlag, New York. 185 pp.

Kullerud, G., Yund, R.A., Moh, G.H., 1969. Phase relations in the Cu–Fe–S, Cu–Ni–S and Fe–Ni–S systems. Econ. Geol. Monogr. 4, 323–343.

Lindstrom, D.J., 1976. Experimental study of the partitioning of the transition metals between clinopyroxene and coexisting silicate liquids. PhD thesis, University of Oregon.

Majzlan, J., Makovicky, M., Makovicky, E., Rose-Hansen, J., 2002. The system Fe–Pt–S at 1100 °C. Can. Mineral. 40, 509–517.

McDonough, W.F., Sun, S.-S., 1995. The composition of the Earth. Chem. Geol. 120, 223–253.

Meisel, T., Walker, R.J., Morgan, J.W., 1996. The osmium isotopic composition of the Earth's primitive upper mantle. Nature 383, 517–520.

Morgan, J.W., Walker, R.J., Brandon, A.D., Horan, M.F., 2001. Siderophile elements in Earth's upper mantle and lunar breccias: data synthesis suggests manifestations of the same late influx. Meteorit. Planet. Sci. 36, 1257–1275.

Murthy, V.R., 1991. Early differentiation of the Earth and the problem of mantle siderophile elements: a new approach. Science 253, 303–306 (and corrections p. 1467).

Neal, C.R., Ely, J.C., Jain, J.C., 2001. The siderophile element budget of the Moon: a reeavaluation, part 2. Lunar and Planetary Science XXXII, Abstract#1662. Lunar and Planetary Institute, Houston. CD-ROM.

O'Neill, H.St.C., Nell, J., 1997. Gibbs free energies of formation of $RuO_2$, $IrO_2$ and $OsO_2$: a high temperature electrochemical and calorimetric study. Geochim. Cosmochim. Acta 61, 5279–5293.

Peach, C.L., Mathez, E.A., Keays, R.R., Reeves, S.J., 1994. Experimentally determined sulfide melt–silicate melt partition coefficients for iridium and palladium. Chem. Geol. 117, 361–377.

Peucker-Ehrenbrink, B., Jahn, B., 2001. Rhenium–osmium isotope systematics and platinum group element concentrations: loess and the upper continental crust. Geochem., Geophys., Geosystems 2, U33–U59.

Rehkämper, M., Halliday, A.N., Fitton, J.G., Lee, D.C., Wieneke, M., Arndt, N.T., 1999. Ir, Ru, Pt, and Pd in basalts and komatiites: new constraints for the geochemical behavior of the platinum-group elements in the mantle. Geochim. Cosmochim. Acta 63 (22), 3915–3934 (NOV).

Robie, R.A., Hemingway, B.S., 1995. Thermodynamic properties of minerals and related substances at 298.15 K and 1 bar (105 pascals) pressure and at higher temperatures. U.S. Geological Survey Bulletin, vol. 2131. U.S. Govt. Printing Office, Washington, DC. 461 pp.

Schmidt, G., Palme, H., 1998. The concentrations of highly siderophile elements in Earth's upper crust as inferred from the compositions of large terrestrial impact melt sheets. Lunar and Planetary Science, vol. XXIX. Lunar and Planetary Institute, Houston. Abstract#1273, CD-ROM.

Schmidt, G., Palme, H., Kratz, K.-L., 1997. Highly siderophile elements (Re, Os, Ir, Rh, Pd, Au) in impact melts from three European craters (Sääksjärvi, Mien and Dellen): clues to the

nature of the impacting bodies. Geochim. Cosmochim. Acta 61, 2977–2987.

Štofko, M., Schmiedl, J., Rosenqvist, T., 1974. Thermodynamics of iron–sulfur–oxygen melts at 1200 °C. Scand. J. Metal. 3, 113–118.

Stone, W.E., Crocket, J.H., Fleet, M.E., 1990. Partitioning of palladium, iridium, platinum and gold between sulfide liquid and basalt melt at 1200 °C. Geochim. Cosmochim. Acta 54, 2341–2344.